Charged Particles on a Two-Dimensional Lattice Subject to Anisotropic Jahn-Teller Interactions

T. Mertelj,[1,2] V. V. Kabanov,[1] and D. Mihailovic[1,2]
[1]*Jozef Stefan Institute, Jamova 39, 1000 Ljubljana, Slovenia*
[2]*Faculty of Mathematics and Physics, University of Ljubljana, Jadranska 19, 1000 Ljubljana, Slovenia*
(Received 12 October 2004; published 14 April 2005)

The properties of a system of charged particles on a 2D lattice, subject to an anisotropic Jahn-Teller-type interaction and 3D Coulomb repulsion, are investigated. In the mean-field approximation without Coulomb interaction, the system displays a phase transition of first order. When the long-range Coulomb interaction is included, Monte Carlo simulations show that the system displays very diverse mesoscopic textures, ranging from spatially disordered pairs to ordered arrays of stripes, or charged clusters, depending only on the ratio of the two interactions (and the particle density). Remarkably, charged objects with an even number of particles are more stable than with an odd number of particles. We suggest that the diverse functional behavior—including superconductivity—observed in oxides can be thought to arise from the self-organization of this type.

DOI: 10.1103/PhysRevLett.94.147003 PACS numbers: 74.20.−z, 74.25.−q, 74.72.−h

The standard theoretical models of strongly correlated electrons, such as the Hubbard model [1] or the $t-J$ model [2], neglect two important interactions, namely, long-range Coulomb repulsion and lattice distortions caused by charged particles. Moreover, these quantum mechanical models are typically used to study $T \approx 0$ properties. As such, these models have found limited applicability in predicting the finite-temperature functional behavior in systems such as cuprate superconductors and other oxides. An important aspect of the problem which has been of great interest recently is the existence of intrinsic mesoscale inhomogeneity in these systems, for which there is mounting experimental evidence from neutron scattering [3], x-ray-absorption fine structure spectroscopy [4], STM [5], and time-resolved carrier dynamics [6] amongst others [7]. There is emerging consensus that in doped cuprates charge carriers may phase segregate to form nanoscale textures. These are believed to be of importance for achieving their functional properties, and particularly superconductivity. The idea of charge segregation in cuprates appeared soon after the discovery of superconductivity [8–10], but in most cases, long-range Coulomb repulsion was not considered. More recently, it was suggested that interplay of short-range lattice attraction and long-range Coulomb repulsion could lead to the formation of short metallic or insulating strings of polarons [11,12]. Since an isotropic interaction cannot lead to stripe formation we suggested instead that an anisotropic mesoscopic Jahn-Teller interaction between electrons and $k \neq 0$ optical phonons might lead to the formation of pairs and stripes [13]. A slightly different approach based on elasticity was considered more recently for the case of manganites by Kugel and Khomskii [14] using the methods of Eremin *et al.* [15] and by Shenoy *et al.* [16]. The importance of the interplay of long-range and short-range forces within an Ising-like model was discussed by Low *et al.* [17] and in a continuous limit by Olson Reichardt *et al.* [18].

The fundamental question which we try to answer here is how charged particles order in the presence of anisotropic Jahn-Teller type interaction, particularly when their density becomes large. We consider charged particles on a 2D square lattice subject to *only* the long-range Coulomb interaction and an anisotropic Jahn-Teller (JT) deformation. In the mean-field (MF) approximation without Coulomb repulsion, the system displays a first order phase transition to an ordered state below some critical temperature. In the presence of Coulomb repulsion, global phase separation becomes unfavorable and the system shows mesoscopic phase separation, where the size of charged regions is determined by the competition between ordering energy and the Coulomb energy. Using Monte Carlo (MC) simulations we show that the system can form many different mesoscopic textures, such as clusters and stripes, depending only on the magnitude of the Coulomb repulsion compared to the anisotropic lattice attraction. Surprisingly, a feature arising from the anisotropy introduced by the Jahn-Teller interaction is that objects with an even number of particles are found to be more stable than with an odd number particles, which could be significant for superconductivity when tunneling is included [19].

Let us consider the JT model Hamiltonian [13], and take only the mode of B_{1g} symmetry:

$$H_{\mathrm{JT}} = g\sum_{\mathbf{r},l} \sigma_{3,l} f(\mathbf{r})(b^{\dagger}_{\mathbf{l}+\mathbf{r}} + b_{\mathbf{l}+\mathbf{r}}), \tag{1}$$

where the Pauli matrix $\sigma_{3,l}$ describes the electronic doublet, g is a constant, and $f(\mathbf{r}) = (r_x^2 - r_y^2) f_0(r)$ where $f_0(r)$ describes the effective range of the interaction [13].

The model is reduced to a lattice gas model by using the adiabatic approximation for the phonon field [14,20]. The Hamiltonian in the pseudospin ($S = 1$) representation is given by:

$$H^{LG}_{\mathrm{JT}-C} = \sum_{\mathbf{i},\mathbf{j}} (-V_l(\mathbf{i}-\mathbf{j}) S^z_{\mathbf{i}} S^z_{\mathbf{j}} + V_c(\mathbf{i}-\mathbf{j}) Q_{\mathbf{i}} Q_{\mathbf{j}}), \quad (2)$$

where $Q_{\mathbf{i}} = (S^z_{\mathbf{i}})^2$, $V_c(\mathbf{m}) = e^2/\epsilon_0 am$ is the 3D Coulomb potential, e is the charge of the electron, ϵ_0 is the static dielectric constant, and a is the effective lattice constant. $S^z = \pm 1$ corresponds to the state with $n_{1,2} = 1$, $n_{2,1} = 0$, and $S^z_i = 0$ to $n_1 = n_2 = 0$. Simultaneous occupancy of both levels is excluded due to the large on-site Coulomb repulsion. The anisotropic short-range attraction is then given by:

$$V_l(\mathbf{m}) = g^2/\omega \sum_{\mathbf{i}} f(\mathbf{i}) f(\mathbf{m}+\mathbf{i}). \quad (3)$$

A similar interaction can also be derived by considering the interaction of the electronic doublet with the strain of B_{1g} symmetry, taking into account St. Venant's compatibility conditions [16]. Anisotropic attraction caused by elasticity has the form [20]:

$$V_l(\mathbf{m}) = -\sum_{\mathbf{k}} \exp(i\mathbf{k}\cdot\mathbf{m}) \frac{g^2}{2[A_2 + A_1 U(\mathbf{k})]}. \quad (4)$$

Here, A_j are the components of the elastic modulus tensor, and $U(k) = \frac{(k_x^2 - k_y^2)^2}{k^4 + 8(A_1/A_2) k_x^2 k_y^2}$. Compared to (3), where the range of the interaction was defined by the coupling to optical phonons, the interaction (4) decays as $1/r^2$ (in 2D) at large distances. Since these attractive forces decay faster than the Coulomb repulsion at large distances, the net potential may have a minimum at short distances.

Our goal is to study the model (2) at constant average density of charged particles, $n = \frac{1}{N}\sum_{\mathbf{i}} Q_{\mathbf{i}}$, where N is the total number of sites. However, to clarify the physical picture we first consider a system with a fixed chemical potential by adding the term $-\mu \sum_{\mathbf{i}} Q_{\mathbf{i}}$ to the Hamiltonian (2).

Models such as (2) but in *the absence of the long-range forces* were previously studied on the basis of the molecular-field approximation [21]. The mean-field equations for particle density n and pseudospin magnetization $M = \frac{1}{N}\sum_{\mathbf{i}} S^z_{\mathbf{i}}$ then have the form [21]:

$$M = \frac{2\sinh(2zV_l M/k_B T)}{\exp(-\mu/k_B T) + 2\cosh(2zV_l M/k_B T)} \quad (5)$$

$$n = \frac{2\cosh(2zV_l M/k_B T)}{\exp(-\mu/k_B T) + 2\cosh(2zV_l M/k_B T)}. \quad (6)$$

Here $z = 4$ is the number of the nearest neighbors for a square lattice in 2D and k_B is the Boltzmann constant. A phase transition to an ordered state with finite M may be of either first or second order, depending on the value of μ. For the physically important case $-2zV_l < \mu < 0$, , ordering occurs as a result of the first order phase transition. The two solutions of Eqs. (5) and (6) with $M = 0$ and with $M \neq 0$ correspond to two different minima of the free energy. The temperature of the phase transition T_{crit} is determined by the condition: $F(M = 0, \mu, T) = F(M, \mu, T)$ where M is the solution of Eq. (5). When the number of particles is fixed [Eq. (6)], the system is unstable with respect to global phase separation below T_{crit}. As a result, at fixed n two phases coexist with $n_0 = n(M = 0, \mu, T)$ and $n_M = n(M, \mu, T)$, resulting in a liquid-gas-like phase diagram (Fig. 1).

To investigate the effects of the long-range forces, we performed MC simulations on the system (2). The simulations were performed on a square lattice with dimensions up to $L \times L$ sites with $10 \leq L \leq 100$ using a standard Metropolis algorithm [22] in combination with simulated annealing [23,24]. At constant n, one MC step included a single update for each site with nonzero Q_i, where the trial move consisted of setting $S_z = 0$ at the site with nonzero Q_i and $S_z = \pm 1$ at a randomly selected site with zero Q_i. A typical simulated annealing run consisted of a sequence of MC simulations at different temperatures. At each temperature the equilibration phase (10^3–10^6 MC steps) was followed by the averaging phase with the same or greater number of MC steps. Observables were measured after each MC step during the averaging phase only. For $L \gtrsim 20$ we observe virtually no dependence of the results on the system size.

Comparing the MC results in absence of Coulomb repulsion shown by t_{crit} in Fig. 1 with MF theory we find the usual reduction of t_{crit} due to fluctuations in 2D by a factor of ~ 2.

Next, we include the Coulomb interaction $V_c(r)$. We use open boundary conditions to avoid complications due to

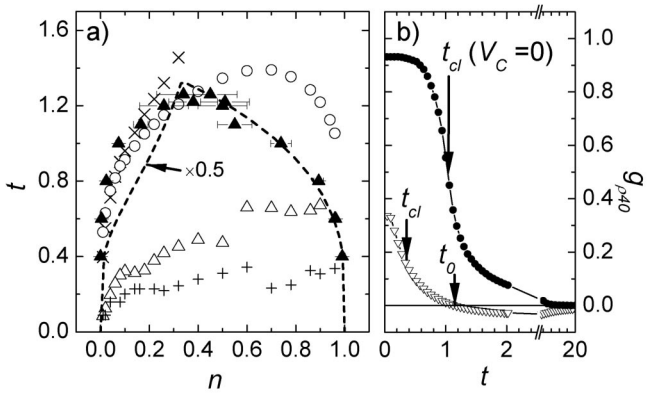

FIG. 1. (a) The phase diagram generated by H_{JT} (2) with and without the Coulomb repulsion (CR). The dashed line is the MF critical temperature, while the full triangles (▲) represent the MC critical temperature, t_{crit}, *without CR*. The open circles (○) represent t_{cl} *without CR*. The open triangles (△) represent t_{cl} while the diagonal crosses (×) represent the onset of clustering, t_0, *in presence of* CR. The cluster-ordering temperature (see text), t_{co}, (also including CR) is shown as crosses (+). The size of the symbols corresponds to the error bars. (b) Typical temperature dependencies of the nearest neighbor density correlation function $g_{\rho L}$ for $n = 0.18$ *in absence of* CR (●) and *in presence of* CR (▽). Arrows indicate the characteristic temperatures.

the long-range Coulomb forces and ensure overall electroneutrality by adding a uniformly charged background electrostatic potential (jellium) to Eq. (2). The short-range potential $v_l(\mathbf{i}) = V_l(\mathbf{i})\epsilon_0 a/e^2$ was taken to be nonzero only for $|\mathbf{i}| < 2$ and is therefore specified only for nearest and next-nearest neighbors as $v_l(1,0)$ and $v_l(1,1)$, respectively.

The anisotropy of the short-range potential has a profound influence on the particle ordering. We can see this if we fix $v_l(1,0) = -1$ at a density $n = 0.2$ and vary the next-nearest neighbor potential $v_l(1,1)$ in the range from -1 to 1. When $v_l(1,1) < 0$, the attraction is "ferrodistortive" in all directions, while for positive $v_l(1,1) > 0$, the interaction is "antiferrodistortive" along the diagonals. The resulting clustering and ordering of clusters at $t = 0.04$ is shown in Fig. 2(a). As expected, a more symmetric attraction potential leads to the formation of more symmetric clusters. On the other hand, for $v_l(1,1) = 1$, the "antiferrodistortive" interaction along diagonals prevails, resulting in diagonal stripes.

In the temperature region where clusters are partially ordered, the heat capacity ($c_L = \partial\langle E\rangle_L/\partial T$ where E is the total energy) displays the peak at t_{co}. The peak displays no scaling with L, indicating that no long-range ordering of clusters appears. Inspection of the particle distribution snapshots at low temperatures [Fig. 2(a)] reveals that finite size domains form. Within domains the clusters are perfectly ordered. The domain wall dynamics seems to be much slower than our MC simulation time scale preventing domains to grow. The effective L is therefore limited by the domain size. This explains the absence of the scaling and clear evidence for a phase transition near t_{co}.

We now focus on the shape of the short-range potential which promotes the formation of stripes shown in Fig. 2(a). We set $v_l(1,0) = -1$ and $v_l(1,1) = 0$ and study the density dependence. Since the inclusion of the Coulomb interaction completely suppresses the first order phase transition at $t_{\rm crit}$, we measure the nearest neighbor density correlation function $g_{\rho L} = \frac{1}{4n(1-n)L^2}\sum_{|\mathbf{m}|=1}\langle\sum_{\mathbf{i}}(Q_{\mathbf{i}+\mathbf{m}} - n)(Q_{\mathbf{i}} - n)\rangle_L$ to detect clustering. Here $\langle\rangle_L$ represents the MC average. We define a dimensionless temperature $t_{cl} = k_B T_{cl}\epsilon_0 a/e^2$ as the characteristic crossover temperature related to the formation of clusters at which $g_{\rho L}$ rises to 50% of its low temperature value. The dependence of t_{cl} on the density n is shown in the phase diagram in Fig. 1. Without Coulomb repulsion $V_c(r)$, t_{cl} follows $t_{\rm crit}$, as expected. The addition of Coulomb repulsion $V_C(r)$ results in a significant decrease of t_{cl} and suppression of clustering. At low densities we can estimate the onset for cluster formation by the temperature, t_0, at which $g_{\rho L}$ becomes positive. It is interesting to note that t_0 almost coincides with the $t_{\rm crit}$ line at low n (Fig. 1).

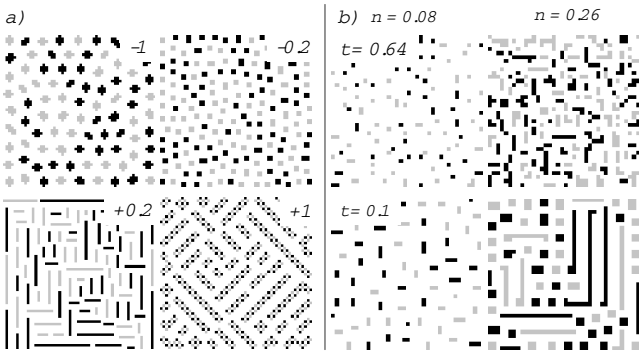

FIG. 2. (a) Snapshots of clusters ordering at $t = 0.04$, $n = 0.2$, and $v_l(1,0) = -1$ for different diagonal $v_l(1,1)$ (given in each figure). Grey and black dots represent particle clusters in state $S_i^z = 1$ and states $S_i^z = -1$, respectively. The preference for even-particle-number clusters in certain cases is clearly observed, for example, for $v_l(1,1) = -0.2$. (b) Snapshots of the particle distribution for two densities at two different temperatures $t = 0.64$ and $t = 0.1$, respectively.

To illustrate this behavior, Fig. 2(b) shows snapshots of the calculated MC particle distributions at two different temperatures for different densities. The growth and ordering of clusters with decreasing temperature is clearly observed. At low n, the particles form mostly pairs with some short stripes. With further increasing density, quadruples gradually replace pairs, then long stripes appear, mixed with quadruples, etc., Around $n \approx 0.5$, stripes prevail forming a labyrinthlike pattern. The density correlation function shows that the correlation length increases with doping, but long-range order is never achieved (in contrast to the case without V_c). Note that while locally there is no fourfold symmetry, the overall correlation function still retains fourfold symmetry.

To get further insight in the cluster formation we measured the cluster-size distribution. In Fig. 3 we show the temperature and density dependence of the cluster-size distribution function $x_L(j) = \langle N_p(j)\rangle_L/(nL^2)$, where $N_p(j)$ is the total number of particles within clusters of size j. At the highest temperature, $x_L(j)$ is close to the distribution expected for the random ordering. As the temperature is decreased, the number of larger clusters starts to increase at the expense of single particles. Remarkably, as the temperature is further reduced, clusters of certain size start to prevail. This is clearly seen at higher densities (Fig. 3). Depending on the density, the prevailing clusters are pairs up to $n \approx 0.2$, quadruples for $0.1 \lesssim n \lesssim 0.3$, etc., We note that for a large range of $v_l(1,0)$, the system prefers clusters with an even number of particles. Odd particle-number clusters can also form, but have a much narrower parameter range of stability [24]. The preference to certain cluster sizes becomes clearly apparent only at temperatures lower then t_{cl}, and the transition is not abrupt but gradual with the decreasing temperature. Similarly, with increasing density, changes in textures also indicate a series of crossovers.

The results of the MC simulation presented above allow quite a general interpretation in terms of the kinetics of first order phase transitions [25]. Let us assume that a single cluster of ordered phase with radius R appears. As was

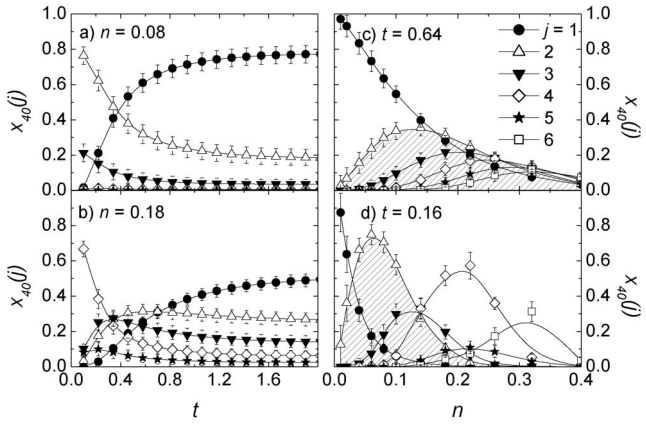

FIG. 3. The temperature dependence of the cluster-size distribution function $x_L(j)$ (for the smallest cluster sizes) as a function of temperature at two different average densities $n = 0.08$ (a) and $n = 0.18$ (b). $x_L(j)$ as a function of n at the temperature between t_0 and t_{cl} (c), and near t_{co} (d). The ranges of the density where pairs prevail are very clearly seen in (d). Error bars represent the standard deviation.

discussed in [13,20,26], the energy of the cluster is determined by three terms: $\epsilon = -F\pi R^2 + \alpha\pi R + \gamma R^3$. The first term is the energy gain due to the ordering phase transition where F is the energy difference between the two minima in the free energy density. The second term is the surface energy parametrized by α, and the third term is the Coulomb energy, parametrized by γ. If $\alpha < \pi F/3\gamma$, ϵ has a well defined minimum at $R = R_0$ corresponding to the optimal size of clusters in the system. Of course, these clusters are also interacting among themselves via Coulomb and strain forces, which leads to clusters ordering or freezing of cluster motion at low temperatures as shown by the MC simulations.

We conclude that a model with only anisotropic JT strain and a long-range Coulomb interaction gives rise to a remarkably rich phase diagram including pairs, stripes and charge- and orbital- ordered phases, of clear relevance to functional oxides. The energy scale of the phenomena is defined by the parameters used in $H_{\mathrm{JT}-C}$ (2). For example, using the measured value $\epsilon_0 \simeq 40$ [27] for La_2CuO_4, we estimate $V_c(1, 0) = 0.1$ eV, which is also the typical energy scale of the ''pseudogap'' in the cuprates. The robust prevalence of the paired state in a wide region of parameters [Fig. 3(c) and 3(d)] is particularly interesting from the point of view of superconductivity. In contrast to Bose condensation of mobile intersite bipolarons discussed by Alexandrov and Mott [28], it has been suggested that pair tunneling between objects such as those shown in Fig. 2 can lead to an insulator-to-superconductor transition [19]. A similar situation occurs in manganites and other oxides with the onset of a conductive state at the threshold of percolation, but different textures are expected to arise from the different magnitude (and anisotropy) of $V_l(\mathbf{n})$ and static dielectric constant ϵ_0 in the different materials [29].

We wish to acknowledge valuable discussions with S. Shenoy, K. Alex Muller, L. P. Gor'kov, A. S. Alexandrov, and A. R. Bishop.

[1] E. Dagotto, Rev. Mod. Phys. **66**, 763 (1994).
[2] J. Jaklic and P. Prelovšek, Adv. Phys. **49**, 1 (2000).
[3] R. J. McQueeney *et al.*, Phys. Rev. Lett. **82**, 628 (1999).
[4] A. Bianconi *et al.*, Phys. Rev. Lett. **76** 3412 (1996); E. S. Bozin *et al.*, Phys. Rev. Lett. **84**, 5856 (2000).
[5] S. H. Pan *et al.*, Nature (London) **413**, 282 (2001); K. McElroy *et al.*, Nature (London) **422**, 592 (2003).
[6] J. Demsar *et al.*, Phys. Rev. Lett. **82**, 4918 (1999); see also a review by D. Mihailovic and V. V. Kabanov, cond-mat/0407204.
[7] See also: D. Mihailovic and K. A. Müller, in *High T_c Superconductivity 1996: Ten Years After the Discovery*, edited by E. Kaldis, E. Liarokapis, and K. A. Müller, NATO Advanced Study Institutes, Ser. E, Vol. 343 (Kluwer, Dordrecht, 1997), p. 243.
[8] J. Zaanen and O. Gunnarsson, Phys. Rev. B **40**, 7391 (1989).
[9] V. J. Emery, S. Kivelson, and O. Zachar, Phys. Rev. B **56**, 6120 (1997).
[10] L. P. Gorkov and A. V. Sokol, JETP Lett. **46**, 420 (1987).
[11] F. V. Kusmartsev, Phys. Rev. Lett. **84**, 530 (2000); **84**, 5026 (2000).
[12] A. S. Alexandrov and V. V. Kabanov, JETP Lett. **72**, 569 (2000).
[13] D. Mihailovic and V. V. Kabanov, Phys. Rev. B **63**, 054505 (2001); **65**, 212508, (2002); J. Supercomput. **13**, 959 (2000).
[14] D. I. Khomskii and K. I. Kugel, Europhys. Lett. **55**, 208 (2001); Phys. Rev. B **67**, 134401 (2003).
[15] M. B. Eremin, A. Yu. Zavidonov, and B. I. Kochelaev, Zh. Eksp. Teor. Fiz. **90**, 537 (1986).
[16] S. R. Shenoy, T. Lookman, A. Saxena, and A. R. Bishop, Phys. Rev. B **60**, R12537 (1999); T. Lookman *et al.*, Phys. Rev. B **67**, 024114 (2003).
[17] U. Löw, V. J. Emery, K. Fabricious, and S. A. Kivelson, Phys. Rev. Lett. **72**, 1918 (1994).
[18] C. J. Olson Reichardt, C. Reichardt, and A. R. Bishop, Phys. Rev. Lett. **92**, 016801 (2004).
[19] D. Mihailovic, V. V. Kabanov, and K. A. Muller, Europhys. Lett. **57**, 254 (2002).
[20] V. V. Kabanov *et al.* (to be published).
[21] J. Lajzerovicz and J. Sivardiere, Phys. Rev. A **11**, 2079 (1975).
[22] N. Metropolis *et al.*, J. Chem. Phys. **21**, 1087 (1953).
[23] S. Kirkpatrick, C. D. Gelatt, and M. P. Vecchi, Science **220**, 671 (1983).
[24] T. Mertelj *et al.* (to be published).
[25] E. M. Lifshitz and L. P. Pitaevski, *Physical Kinetics* (Butterworth-Heinemann, Washington, DC, 1980), Ch. 12.
[26] L. P. Gorkov, J. Supercond. **14**, 365, (2001).
[27] D. Reagor *et al.*, Phys. Rev. Lett. **62**, 2048 (1989).
[28] A. S. Alexandrov and N. F. Mott, *Polarons and Bipolarons* (World Scientific, Singapore, 1995).
[29] E. Dagotto, T. Hotta, and A. Moreo, Phys. Rep. **344**, 1 (2001).